Progress in Organic Coatings 96 (2016) 42–51

Contents lists available at ScienceDirect

Progress in Organic Coatings

journal homepage: www.elsevier.com/locate/porgcoat

Development of hybrid sol–gel coatings for the improvement of metallic biomaterials performance

M.J. Juan-Díaz[a], M. Martínez-Ibáñez[a], I. Lara-Sáez[b], S. da Silva[b], R. Izquierdo[b], M. Gurruchaga[a], I. Goñi[a], J. Suay[b,*]

[a] Facultad de Ciencias Químicas, Universidad del País Vasco, P. M de Lardizábal, 3, San Sebastián 20018, Spain
[b] Departamento de Ingeniería de Sistemas Industriales y Diseño, Universidad de Castellón, Av. Sos Baynat s/n, Castellón 12071, Spain

ARTICLE INFO

Article history:
Received 9 June 2015
Received in revised form 7 January 2016
Accepted 25 January 2016
Available online 2 February 2016

Keywords:
Sol–gel hybrid coatings
Si release
Osteoinductive ability

ABSTRACT

Ti implants osteointegration is widely recognized. However, silicon deficiency in animals leads to bone defects, since this element plays an important role in bone metabolism. Thus, hybrid (organic–inorganic) sol–gel coatings synthesis has been performed to create a material able to release silicon compounds under *in vivo* conditions, to promote a fast and good osseointegration. Synthesis procedures included acid-catalysed hydrolysis, *sol* preparation and the subsequent gelation and drying. To this end, methyl-trimethoxysilane (MTMOS) and 3-glycidoxypropyl-trimethoxysilane (GPTMS), alkoxide precursors with different molar ratios were used. After the determination of the optimal synthesis parameters to obtain homogeneous films, the materials were physicochemically characterized by ^{29}Si nuclear magnetic resonance (^{29}Si NMR), Fourier transform infrared spectroscopy (FT-IR), contact angle measurements and electrochemical impedance spectroscopy (EIS) tests. The materials were assayed *in vitro* for their ability to release Si in a controlled manner. The sustained release of Si over long periods was demonstrated. Electrochemical analysis revealed the formation of pores and water uptake during the degradation. The degradation kinetics and Si release of coatings was mainly influenced by the amount of GPTMS. Among the cell types involved in bone regeneration, human adipose tissue-derived mesenchymal stem cells (AMSCs) are included; thus, the attachment and proliferation of these cells onto the coatings was analyzed. Furthermore, the osteoinduction capacity of the coatings was evaluated by establishing the mineralized extracellular matrix production by quantification of calcium-rich deposits. MSCs had good cell proliferation onto the hybrid coatings and could be able to produce mineralized extracellular matrix, evidencing an active osteoinduction process. After the *in vitro* tests, one formulation was selected to coat titanium implants and perform an *in vivo* test in rabbits. Although the *in vivo* results were not as good as those obtained *in vitro*, we demonstrated that the ability to utilize sol–gel coating processes on titanium implants opened up the opportunity to tailor surfaces to clinical requirements. Thus, a further research is proposed to include other precursors that enhance the coating degradation kinetics in order to obtain an early release of Si compounds that accelerate the osseointegration.

1. Introduction

The *sol–gel* technique has been used over the last decade to prepare functional hybrid materials for biomedical applications [1,2]. Among the characteristics that make it interesting in the biomaterials field, we can emphasize the versatility of the sol–gel process to coat different surfaces with complex shapes, good adhesion to many types of surfaces, biodegradability and biocompatibility. An interesting application of these types of materials is to use them to release silicon compounds from the hydrolytic degradation of the *sol–gel* matrix [3]. The major advantage of these materials is that the library of methods and chemicals with which one can design almost any desired surface property is practically endless (*i.e.* the degradation kinetic). One interesting siloxane precursor is the 3-glycidoxypropyl-trimethoxy-silane (GPTMS) due to the oxirane ring that provides a functional and reactive group. GPTMS has been previously studied and proved to be a component able to give non-cytotoxic hybrid materials or scaffolds, which can stimulate bone cell proliferation [4,5].

In 1972, Carlisle [6] and Schwarz and Milne [7] first reported that silicon deficiency in chicks and rats led to abnormally shaped bones and defective cartilaginous tissue, both of which were restored

* Corresponding author.
E-mail address: suay@esid.uji.es (J. Suay).

http://dx.doi.org/10.1016/j.porgcoat.2016.01.019
0300-9440/

upon the addition of soluble Si to their diet. This led to the suggestion that Si may play an important role in connective tissue metabolism especially in bone and cartilage [8].

Studies *in vitro* of the effects of soluble Si on human osteoblasts have been done using Zeolite A (ZA), which is a silicon-containing compound. Keeting et al. [9] showed that ZA stimulated the proliferation and differentiation of cultured cells of the osteoblast lineage. Others studies demonstrated how the orthosilicic acid stimulates collagen type 1 synthesis and osteoblastic differentiation [10], showing the influence of Si in the activity of bone cells [11], and improving the formation of bone nodules [12].

When bone regeneration is needed (*i.e.* the use of a dental implant), mesenchymal stem cells play the major role. When the cells attach onto the surface of prostheses, they can drastically accelerate the integration of the implant [13], since they can differentiate into osteoblastic cells, which start the formation of new bone [14]. It is well known that many reasons for excluding patients from dental implant treatment are mainly due to their bone quality. Consequently, dental implant that will lead to better and faster osseointegration and provide enduring stability is the key to reduce the cohort of excluded potential implant users.

The present study reports on the synthesis *via* sol–gel method of hybrid (silica and organic chains) networks with a mixture of two alkoxysilanes, GPTMS and methyl-trimethoxysilane (MTMOS), in different molar proportions. The aim of the work is to investigate how changes in composition of the hybrid network influence the degradation of the matrix and further the release of silicon compounds, and its effect on the proliferation and mineralization of MSCs. In order to characterize the network formation, physicochemical analysis was performed by FTIR and RMN. The electrochemical impedance spectroscopy (EIS) technique was used to study the initial pore structure of the materials and further changes in the coating because of degradation, fundamentally assessing its capacity to resist pore formation and water uptake, recording both parameters as a function of time. Furthermore, all these results together with those of the *in vitro* tests allowed us to choose one formulation to be applied as a coating on Ti dental implants and be tested *in vivo*.

2. Materials and methods

2.1. Materials

a) *Sol–gel* synthesis

Organic–inorganic hybrids coatings were synthesized from MTMOS (Sigma–Aldrich) and GPTMS (Sigma–Aldrich). The molar ratios MTMOS:GPTMS used were 10:0, 8:2, 5:5, 2:8 and 0:10, giving rise to coatings named: MTMOS, 8M:2G, 5M:5G, 2M:8G and GPTMS. In all cases, 2-propanol was used as co-solvent to obtain a miscible solution of the siloxanes, the volume ratio alcohol:siloxane was defined as 1:1 and the stoichiometric amount of acidified water as the catalyst of the reaction. The acid water was prepared by mixing distilled water with 0.1 N HNO_3 until pH arrives to 1. Solutions were stirred for about 1 h and set for another hour at room temperature before their deposition on the Petri dishes by solvent casting.

Three types of samples were obtained for the characterization: coatings deposited on a metal substrate, coatings on a glass disc, and free films (non-adherent to a substrate).

b) Substrate preparation and *sol* deposition

Petri dishes (Afora) were used as glass substrate for *sol–gel* deposition after cleaning in an ethanol bath ultrasonicated for 5 min with a power of 30 W using Sonoplus HD 3200, followed by distilled water rinsing, soaking in ethanol and, finally, dried at 150 °C. Afterwards, to improve wettability, the glass Petri dishes were activated with an Argon plasma treatment (200 sccm) during 30 s (Plasma-Electronic PICCadheredOLO, 50 Pa, 300 W). After this treatment, a drop of sol of 10 μl was flowed horizontally to obtain a homogenous coating in the glass surface. The thermal curing of the coatings was optimized until homogeneous films, free of cracks and transparent, were obtained.

Table 1
Thermal curing applied to the coatings and its conditions.

Formulation	MTMOS	GPTMS	MTMOS:GPTMS
Cure temperature (°C)	100	140	140
Cure time (min)	120	120	120

Stainless steel AISI 316-L plates (5 cm × 5 cm, RNSinox, S.L.) were used as metal substrate for *sol–gel* deposition. The plates were cleaned with acetone to remove impurities and oil. A dipping device (KSV instrument-KSV DC) with a controlled withdrawal speed was used for the film deposition. Plates were immersed into the solution at a speed of 100 mm min^{-1}, left for 1 min and then removed at the same speed.

In order to obtain a free *sol–gel* film, Teflon moulds were used. An appropriate quantity of *sol* was poured into the mould to obtain a homogeneous final film that was carefully removed.

The thermal process applied for all cases is described in Table 1.

2.2. Chemical characterization

^{29}Si NMR solid spectroscopy was used to determine the Si—O—Si cross-linking density after curing treatment. Spectra were recorded on a Bruker 400 AVANCE II WB PLUS spectrometer, equipped with a CP-MAS (Cross Polarization Magic Angle Spinning) probe. The samples were placed in a rotor sample tube of 4 mm. The sample spinning speed was 7.0 kHz. The pulse sequence used was the Bruker standard, frequency 79.5 MHz, spectral width 55 KHz, contact time 2 ms and delay time 5 s.

The structure of the hybrid coatings was examined by Fourier-transform infrared (FTIR) spectroscopy (Model FTIR 6700, NICOLET). The spectra were recorded on the attenuated total reflectance (ATR) mode and the wavelength range was between 4000 and 400 cm^{-1}.

2.3. Contact angle

The contact angle of deionised water on the different coatings was measured using an automatic contact angle meter (OCA20 Goniometer). The wettability of the coatings (deposited on stainless steel AISI 316-L) was determined by the half angle method. A sessile drop of 10 μl of deionised water was placed on the coated surfaces. The value given is the mean value of at least 11 measurements.

2.4. Si release assay

Si release was studied by the immersion of the coatings deposited on a glass substrate in 50 ml of Milli-Q water and kept at 37 °C for 5 weeks. Sample was taken once a week. The release was determined using an ICP-MS (Inductively coupled plasma mass spectrometry) Instrument Agilent 7700 Series. Each data point is the average of three individual measurements.

2.5. Electrochemical impedance spectroscopy (EIS)

Electrochemical impedance spectroscopy tests were carried out on coated samples (3.2 ± 0.7 mm thickness) deposited on the metallic substrate exposed to 3.5% NaCl (by weight) in deionised water for up to 24 h. A three electrode electrochemical cell was

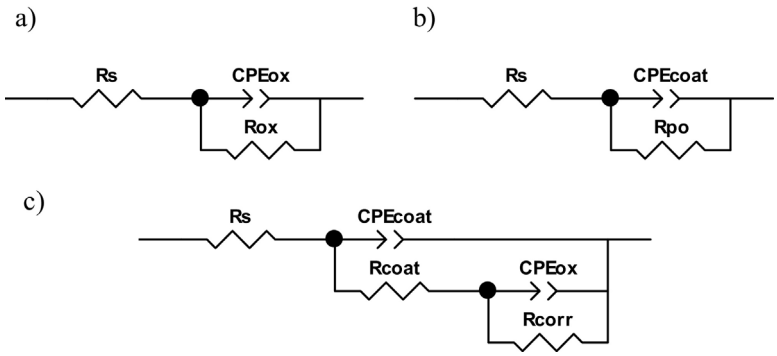

Fig. 1. Equivalent circuit employed to model (a) stain steel substrate and (b) and (c) sol gel coatings applied over the metallic substrate.

obtained by sticking a glass cylinder onto the sample sheet and filling it with the test solution.

The exposed surface area was 3.14 cm^2. A carbon sheet acted as the counter-electrode and an Ag/AgCl electrode was used as the reference electrode. The AC impedance data were obtained at the free corrosion potential using an IM6/6eX Zahner-elektrik potentiostat and a frequency response analyser. The impedance tests were carried out over a frequency range of 100 kHz down to 10 mHz using a sinusoidal voltage of 10 mV as the amplitude inside a Faraday cage. This was in order to minimize external interferences on the system. The impedance spectra were analyzed using Z-view software and three different equivalent circuit models, as shown in Fig. 1. The first model (Fig. 1a) consists on an equivalent electric circuit with the solution resistance (R_S) in series with the capacitive–resistive elements (CPE_{ox} and R_{ox}) in parallel representing the metal oxide and its resistance for a stainless steel substrate. For fitting the sol gel coatings behaviour when they are applied over the metallic substrate, the equivalents circuits represented in Fig. 1a and b can be used depending on the quality of the sol gel film. CPEcoat represents the leaking capacitor modelling the coating and R_{po} representing the resistance of the electrolyte when pass through the pores of the hybrid layer [15,16]. The Chi-squared parameter of the fit was always below 0.01. Fitting the EIS data to the circuits determines the values of the characteristic parameters of the equivalent circuit, which are generally assumed to be related to the corrosion properties of the system [17]. Fitting the impedance data to the parameters of the first time constant of the circuit (high frequencies) allows the parameters R_{po} and C_c to be obtained. R_{po} can be related to porosity and the deterioration of the coating while C_c is related to the water absorption and coating degradation [18,19]. When modelling the equivalent circuit with CPE, the software gives values of capacitance in s^n/Ω units together with a parameter known as "n". When n is close to 1 (ideal capacitor), as was the case in this study, it can be considered that the values of capacitances given by the software match with the effective capacitances (ideal).

It is generally assumed that the elements of the equivalent circuits are correlated to the corrosion properties of the system [15,20]. Although it is necessary in order to fit correctly the equivalent circuit to all impedance spectra *versus* frequency, this study is only related to the characterization of the hydrolysis degradation of the sol–gel coating. For this reason, we will focus our attention on those results obtained at high frequency, where the response of the coating to electrolyte exposition (parameters of the equivalent circuit R_{po} and C_c) is located.

2.6. Biological characterization

2.6.1. In vitro *tests. Assays with MSCs*

The biocompatibility and the osteoinduction of the coatings were tested with human adipose tissue-derived mesenchymal stem cells (AMSCs). To perform the cell culture onto the samples, the *sol–gel* coatings were deposited on a glass substrate and sterilized by 30 min exposure to UV in a tissue culture cabin. All samples were preconditioned overnight dipping in Dulbecco's Modified Eagle's Medium (DMEM-Glutamax) (Gibco) to ensure protein adsorption.

To perform cell adhesion and proliferation assay about 12500 cells/cm^2 were seeded onto the sample surfaces and incubated during 14 days at 37 °C in 5% CO_2/air atmosphere. Proliferation of cells was measured by analyzing the mitochondrial activity using a colorimetric cell proliferation test kit (MTT, Roche) at different culture times (0, 7 and 14 days). The absorbance was measured with a Multiskan Ascent plaque reader at $\lambda = 550$ nm. The experiments were performed in triplicate.

In order to analyze the osteoinduction capacity of the coatings, the calcium deposits formed by cells in an osteogenic culture medium were measured using Alizarin Red S staining. To perform the assay, about 2000 cell/cm^2 were seeded onto the surface and incubated in DMEM-Glutamax containing 10% FBS during 7 days at 37 °C in 5% CO_2/air atmosphere. Then, the culture medium was changed into an Osteoblast Differentiation Medium (Gibco) and incubated during 14 days, changing the medium every 72–96 hours. Finally, the calcium deposits were quantified using 2% Alizarin Red (Sigma–Aldrich) pH 4.1–4.3. The absorbance was measured with a Multiskan Ascent plaque reader at $\lambda = 570$ nm.

2.6.2. In vivo *test. Experimental design and animal model*

Titanium dental screws covered with the sol–gel coating were implanted in rabbit proximal tibia. All procedures followed the Rules of Ethical Committee in University of Murcia (Spain) and the European Directive. Both tibiae of twenty male and female rabbits (New Zealand white) with an average weight of 2–3 kg were used. The animals were individually housed and kept in a controlled animal room with a 12 h light/dark cycle at 20.5 ± 0.5 °C and 45–65% of relative humidity. Animals were fed with a standard diet and filtered tap water *ad libitum*. One control sample (uncoated screw) and one 5M:5G coated screw were implanted per animal in opposite tibiae. Finally, surgical sites were closed in layers. Injury was washed with saline solution and was covered with a plastic spray dressing (Nobecutan®, Inibsa Laboratories, Barcelona; Spain). The animals were randomly divided into four experimental period groups of 1, 2, 4 and 8 weeks after implantation, five animals per study and period were implanted. Rabbits were euthanized with carbon monoxide inhalation at the end of the corresponding time. Three of the five samples per period were processed for its histological analysis with light microscope. The other samples were processed for studying coating degradation and Si release by scanning electron microscope (SEM) images and EDX (energy-dispersive X-ray spectroscopy) microanalysis.

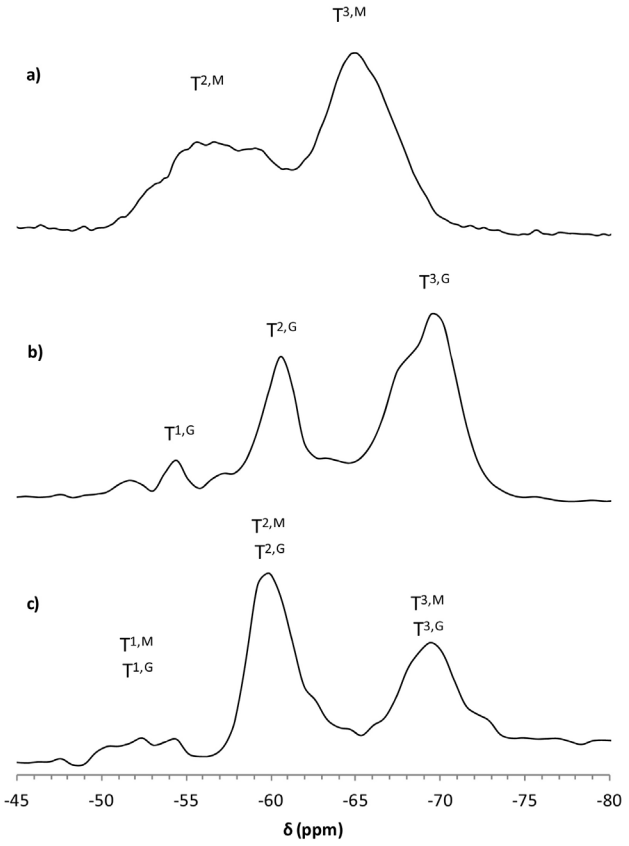

Fig. 2. ^{29}Si solid NMR spectra of (a) MTMOS, (b) GPTMS and (c) 5:5 MTMOS:GPTMS.

2.6.3. In vivo *test. Histological examination*

Non-decalcified tibia sections with titanium screw were processed for histological examination as described in the literature [21]. The samples embedded in polymethyl methacrylate (PMMA) blocks were sectioned into 25–30 mm thick slices using an EXAKT® technique (EXAKT Technologies, Inc., Oklahoma; USA) and sections were stained using Gomori Trichrome stain. Slides were examined under light microscope.

2.6.4. In vivo *Si release*

Samples obtained after euthanasia were immediately transferred to glutaraldehyde 2.5% (Sigma–Aldrich, Missouri; EEUU) in 0.1 M phosphate buffer (PB). Samples were processed as described by other authors [22]. Carbon coated samples were observed in a scanning electron microscope (LEO440i, Leica, Heerbrugg; Switzerland) equipped with a BSE (Backscattered Electrons) detector and an Oxford INCA EDX microanalysis (Oxford Technologies, Oxfordshire, UK) with 20 kV high tension conditions.

3. Results and discussion

3.1. Chemical characterization

A reaction time of 2 h was needed to obtain a *sol*, after hydrolysis and condensation processes, with an appropriate viscosity to permit the film deposition on the substrates. Then, a thermal treatment was carried out to obtain a solid film by promoting cross-linking and solvent evaporation. Different conditions were applied in order to get good quality coatings (homogeneous and without pores); the final conditions are given in Table 1.

Table 2
^{29}Si solid chemical shift (δ) for MTMOS, GPTMS and 5M:5G.

Formulation	Chemical shifts δ (ppm)		
	T^1	T^2	T^3
MTMOS (T^M)		−50 to −65	−60 to −71
GPTMS(T^G)	−50 to −56	−53 to −63	−64 to −75
5M:5G (T)	−48 to −56	−57 to −69	−64 to −75

Table 3
Percentage abundance of silicon species and Si—O—Si network connectivity for MTMOS, GPTMS and 5M:5G.

Formulation	T^1	T^2	T^3	Dc (%)
MTMOS	–	40	60	86.7
GPTMS	3	35	62	86.3
5M:5G	0	48	52	84.0

Fig. 2 represents the ^{29}Si solid NMR spectra of MTMOS, GPTMS and 5:5 MTMOS:GPTMS after the thermal treatment. The degree of condensation of each precursor and the network connectivity was studied. Table 2 summarizes the ^{29}Si chemical shift for the different species of each precursor and the mixture 5M:5G as an example.

The MTMOS spectrum shows T^2 and T^3 signals, with a higher intensity of T^3. The solid obtained with GPTMS shows signals associated to T^1, T^2 and T^3, where the intensity of T^1 is the lowest and the highest the one of T^3. The MTMOS:GPTMS spectrum shows signals of T^1, T^2, the one with highest intensity, and T^3. The fact that in the mixture the most abundant specie was the T^2 and not the T^3, is due to the slower progress of the reactions in the liquid medium of the mixtures than the progress of the reactions of the pure precursors. Thus, precursors mixtures give a less crosslinked network. This can be due to the steric hindrance caused by the organic groups of both precursors that hindered the evolution of the reaction.

Peak fitting of every spectrum was done, allowing the quantification of each of the silicon species present in hybrids. Furthermore, the degree of condensation (Dc), or connectivity, was determined from the previously calculated percentage values of T species according to the method explained by Mahony et al. [23] (Table 3).

These values show the areal rate of the different formulations proving the previous mentioned decrease in the case of 5M:5G, where a less cross-linked network (Dc) and hence a lower number of Si—O—Si links is obtained.

Fig. 3 shows the FTIR spectra of the films obtained with MTMOS and GPTMS. For both samples, there are two pronounced bands appearing at 1100 cm^{-1} and 1010 cm^{-1} with another one at 790 cm^{-1}, corresponding to the vibration absorption of Si—O—Si groups, indicating that all the samples were mainly composed of silica network.

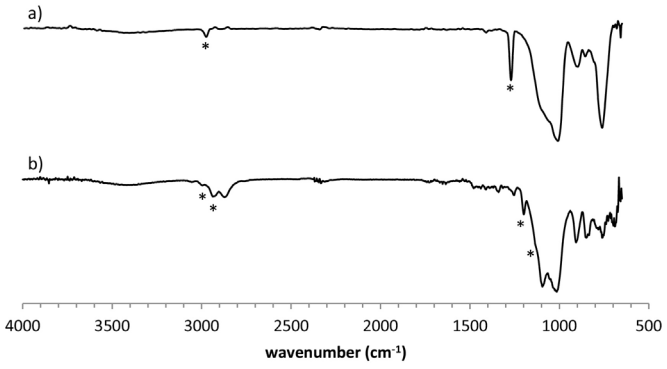

Fig. 3. FTIR spectra of (a) MTMOS and (b) GPTMS films.

Table 4
Representative bands of each precursor.

Formulation	Wave number (cm^{-1})	Assignment
MTMOS	2960	—CH_3
	1275	Si—CH_3
GPTMS	3006	Epoxy ring
	2950	—CH_2—
	1205	Epoxy ring
	1150	CH_2—O—CH_2

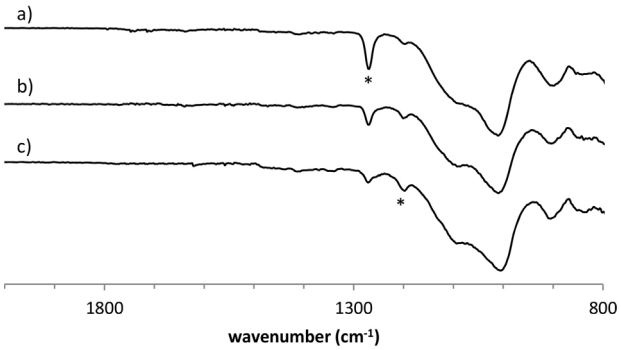

Fig. 4. FTIR spectra of (a) 8M:2G, (b) 5M:5G, (c) 2M:8G films.

Table 5
Water contact angle results with different molar ratios MTMOS:GPTMS deposited on a metal substrate.

Formulation	Wetting contact angle (°)
MTMOS	75.9 ± 1.6
8M:2G	76.6 ± 0.6
5M:5G	66.9 ± 2.0
2M:8G	68.4 ± 2.1
GPTMS	64.8 ± 2.0

As expected, due to the organic groups, which are not involved in the hydrolysis and condensation reactions, characteristic bands of each precursors are developed in the spectra (the asterisked ones). In Table 4, these representative bands of each precursor are described. For the MTMOS coating, the band appearing at 1275 cm^{-1} confirmed the presence of the methyl group. In the case of GPTMS coating the band lying at 1205 cm^{-1} was due to the glycidoxypropyl group. This clearly demonstrated the successful modification of the silica network by those organic groups.

The materials with different molar ratios MTMOS:GPTMS (Fig. 4) maintain the characteristic bands of the precursors alone, the differences in the concentration is confirmed with the intensity change in the bands at 1275 cm^{-1} of MTMOS and the ones of 1205 cm^{-1} and 3006 cm^{-1} associated with the GPTMS.

3.2. Contact angle

The values of the contact angle for the set of materials obtained are summarized in Table 5.

The GPTMS coating is more hydrophilic than the MTMOS coating, this fact is due to the organic groups present in the polysiloxane network, *i.e.* the hydrophilic glycidoxypropyl group of GPTMS and the hydrophobic methyl group of MTMOS. The materials with different molar ratios MTMOS:GPTMS showed contact angle values between those of MTMOS and GPTMS films. This range of values is important since most literature suggests that protein adsorption that leads to a good biocompatibility tends to occur more favourably on hydrophobic surfaces or on surfaces with an intermediate wettability (60–90°) [24].

3.3. Electrochemical impedance spectroscopy (EIS)

The EIS test was performed to study the isolating properties of the coatings along the time in an electrolyte. Samples of stainless steel AISI 316L plates and samples of MTMOS, 8M:2G, 5M:5G, 2M:8G and GPTMS obtained by dip-coating and applied on the stainless plates were used. Fig. 5 shows the Bode and Nyquist graphs of the impedance evolution with time over 24 h for coatings with different molar ratios MTMOS:GPTMS.

Impedance spectra show that MTMOS' impedance values are higher than those obtained in coatings with GPTMS. As the quantity of GPTMS increases the impedance module decreases. This change in MTMOS impedance results at 24 hours is due probably to the higher permeability of the film when the GPTMS is incorporated.

Impedance experimental results for the coatings were modelled according to the proposed equivalent circuits (Fig. 1). A good fit was obtained for all coatings over the complete range of frequencies as is shown in Fig. 6. In the case of MTMOS coatings, only one time constant was detected in the impedance response for short exposure times (model shown in Fig. 1b). However, the coating resistance decreased and the second time constant related to the oxide layer of the substrate appeared after 24 hours in contact with the solution. Two time constants were detected for coatings in the presence of GPTMS (Fig. 1c). This is attributed to a higher permeability in GPTMS coatings that lead to consider the second time constant related to the oxide of the metal. This fact was reflected by the significant decrease of the impedance modulus value for GPTMS' coatings when they are compared to the registered MTMOS impedance.

The aim of this study is to understand how the electrolyte exposure affects the material degradation. In this sense, the discussion is focused only on the first time constant parameters (R_{po} and C_c), which are related to the coating behaviour. Fig. 7 shows Pore Resistance and Fig. 8 Coating Capacity parameters obtained from the response at high frequencies of all coatings.

Pore resistance R_{po} is a measure of the porosity and deterioration of the coating. R_{po} values have usually been related to the number of pores or capillary channels perpendicular to the substrate surface through which the electrolyte reaches the interface [25]. Although the R_{po} can also increase with immersion time, probably as a result of pore or defect blockage by corrosion products, it usually decreases (Fig. 6). Some authors have found three regions in the time dependent trend of R_{po}. It initially decreases rapidly, then slowly (displaying a plateau) and then again rapidly, coinciding with the appearance of the second semicircle. The plateau is explained by making the assumption that the number of pathways formed is approximately constant with time. Thus, it can be said that R_{po} value is a measure of the ionic resistance through the pores of the coatings and is inversely proportional to the extent and number of defects in the coating. The evolution of R_{po} with the exposure time in the electrolyte gives information about the coating capacity to avoid the formation of pores across the film due to its degradation. High and constant R_{po} values are attributed to coatings that do not degrade during electrolyte exposure.

Fig. 7 clearly shows that coatings with GPTMS have values of R_{po} ranking from 3 to 4 magnitudes order being correlated to the increase of its content. GPTMS containing coatings showed less resistance to the flow of water through the coating than in the case of MTMOS coating. The water is able to penetrate the coatings formulated with GPTMS much more than in MTMOS coating, possibly because of their bigger value of hydrophilicity and because they present less condensed networks. On the other hand, if we compare MTMOS:GPTMS coatings with the GPTMS one, we can say that differences in R_{po} are due to heterogeneous porosity in mixture coatings. In these matrixes the MTMOS domains present smaller

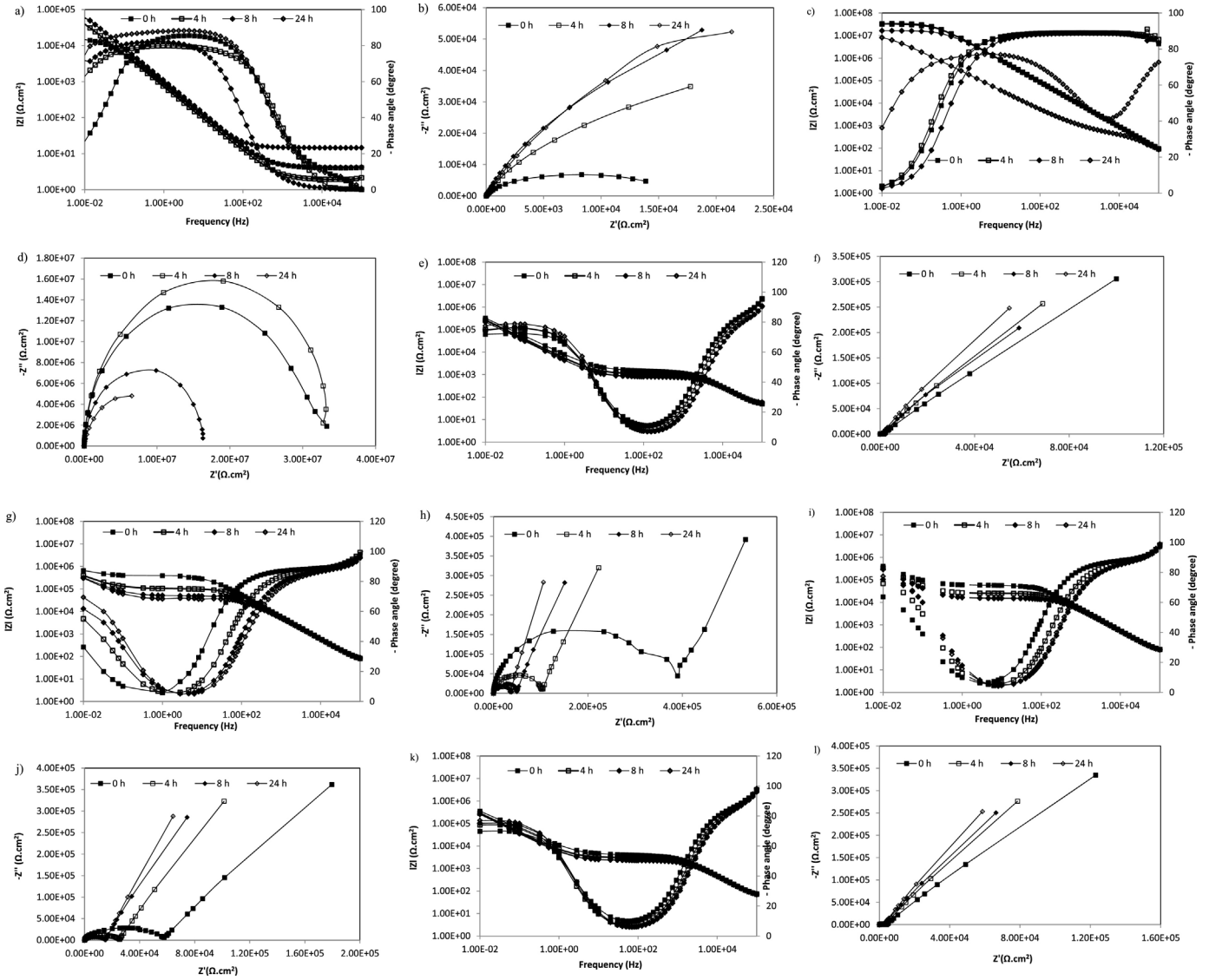

Fig. 5. Evolution of Bode plot for (a) stainless steel, (c) MTMOS, (e) GPTMS, (g) 8M:2G, (i) 5M:5G, (k) 2M:8G and evolution of Nyquist plot for (b) stainless steel, (d) MTMOS, (f) GPTMS, (h) 8M:2G, (j) 5M:5G and (l) 2M:8G coatings during 24 h immersion in electrolyte (deionized water 3.5% NaCl by weight).

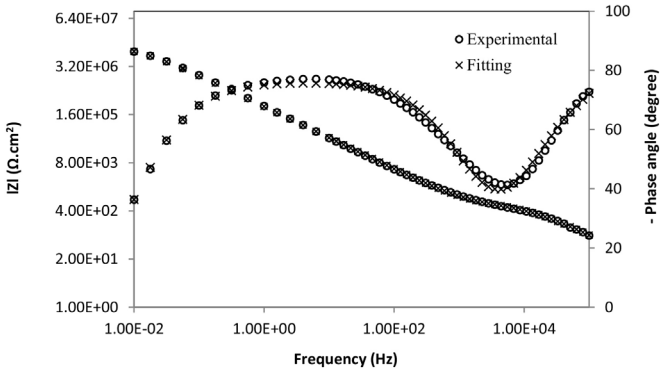

Fig. 6. Bode plot comparison between experimental (*o*) and modelled results (*x*) obtained for the MTMOS coating after 24 h of immersion in electrolyte (deionized water with 3.5% NaCl by weight).

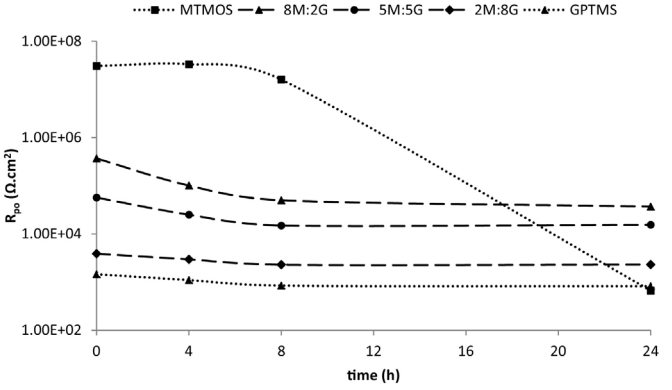

Fig. 7. Evolution of a pore resistance R_{po} *versus* time of exposure to electrolyte (deionized water 3.5% NaCl by weight) for MTMOS, GPTMS, 8M:2G, 5M:5G and 2M:8G coatings.

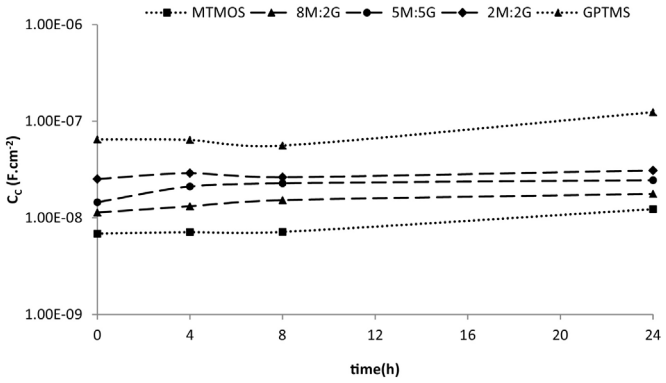

Fig. 8. Evolution of coating capacitance C_c *versus* time of exposure to electrolyte (deionized water 3.5% NaCl by weight) for MTMOS, GPTMS, 8M:2G, 5M:5G and 2M:8G coatings.

porosity than the GPTMS domains, which is reflected in higher R_{po} values for MTMOS than for GPTMS.

On the other hand, C_c is the capacitance of the coating and it is a measure of the water permeation into the coating according to the following expression:

$$C_C = \varepsilon \cdot \varepsilon_0 \cdot \frac{A}{d} \quad (1)$$

where ε is the dielectric constant of the coating, ε_0 the permittivity of vacuum, A the area of the coating exposed to the electrolyte, and d is the thickness. The coating capacitance will usually change (increase) due to electrolyte absorption because the dielectric constant of water is approximately 5 times greater than that of a typical coating.

Fig. 8 shows that C_c values of MTMOS sample are lowest of the series (7×10^{-9} F cm^{-2}) while the values of pure GPTMS are slightly higher. When MTMOS and GPTMS are combined in different ratios a relative intermediate behaviour can be observed. However there is not a direct relationship between the coating capacitance and the amount of GPTMS incorporated. What can be said is that when we start to incorporate GPTMS to the formulation, the water uptake increase due to its molecular properties of this component. Nevertheless this phenomenon is conditioned to the interaction of both components (GPTMS and MTMOS).

All series presented are quite stable through exposure time meaning that there is little variations in the absorption of electrolyte. This behaviour is due to the physicochemical properties of the sol–gel coating that does not allow a large entry of electrolyte in the matrix.

3.4. Si release

The dissolution of various forms of solid silica in aqueous solutions has been the focus of several studies [3]. Furthermore, the compounds that these materials release during their degradation process, mostly orthosilicic acid derivatives ($Si(OH)_3R$), interfere positively in cells activity. In this way, in order to determine the silicon compounds release from the coatings degradation, silicon concentration measurements were carried out. Fig. 9 shows the release curves as a function of the composition of the coatings.

MTMOS coating showed the minimum Si release (less than 2 ppm), while the MTMOS:GPTMS coatings showed a Si release dependent on GPTMS content; the more the GPTMS content in the formulation the more Si released. The coatings 5M:5G and 2M:8G showed same tendency, a fast release during the first two weeks and then an increase up to 7 Si ppm for 5M:5G and 9 ppm for 2M:8G. In the case of 8M:2G the behaviour is more similar to that of MTMOS coating showing a slow release up to 3 Si ppm at the end of the test.

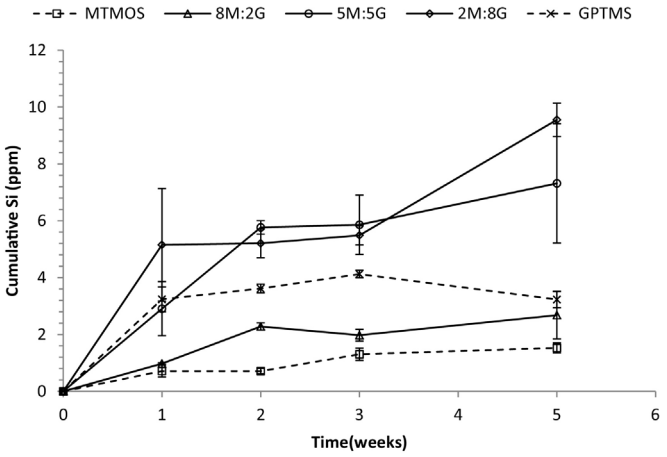

Fig. 9. Silicon compounds release *versus* time of exposure to Mili-Q water at 37 °C for MTMOS, GPTMS, 8M:2G, 5M:5G and 2M:8G coatings.

Additionally, it is interesting to observe that the coatings 2M:8G and 5M:5G, release more Si than the GPTMS one. This phenomenon can be related to the network structure that in the case of GPTMS shows the biggest T^3 species content, while in the other two cases the main specie is T^2, what means a less crosslinked network.

3.5. *Biological characterization.* In vitro *assays with AMSCs*

The aim of these assays is to evaluate the changes in AMSCs behaviour, proliferation and mineralization, as GPTMS content is increased in the coating.

Fig. 10 shows the AMSCs proliferation after seeding them on MTMOS, 8M:2G, 5M:5G, and 2M:8G coatings.

The results show that MTMOS coating presents the worst growth of cells from the beginning of the experiment, showing low values of mitochondrial activity (0.016 a.u.), which did not significantly increase with culture time. When GPTMS is added to the formulation the cell attachment and their proliferation are enhanced. Coating 8M:2G had an improved cell attachment compared with MTMOS (0.054 a.u.) and it shows a slightly increase during the culture, reaching values near 0.15 a.u. Coatings 5M:5G and 2M:8G present the maximum values of mitochondrial activity because they have a progressive improvement in cell proliferation of MSCs until 7 days (0.267 a.u.). Above 7 days the values of mitochondrial activity decreased in both cases.

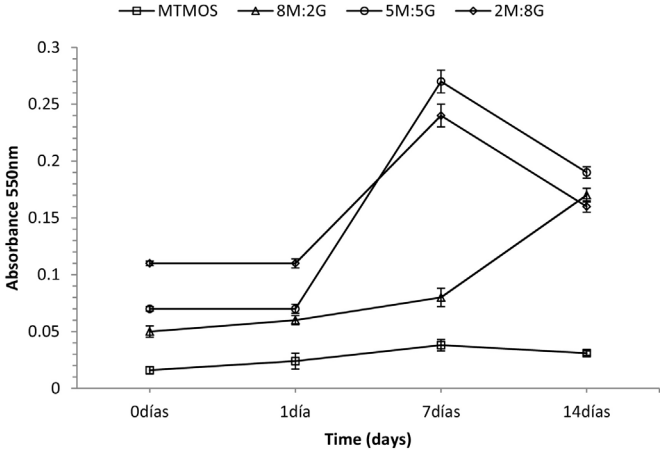

Fig. 10. AMSCs proliferation curves on uncoated glass and coatings surfaces (MTMOS, 8M:2G, 5M:5G, 2M:8G). Measure absorbance at 550 nm.

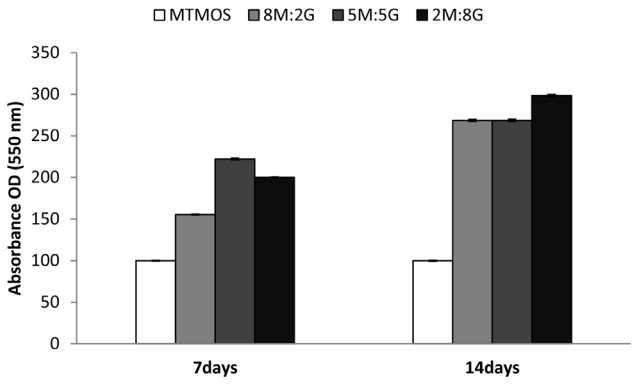

Fig. 11. Alizarin Red S staining at 7 and 14 days on coatings surfaces (MTMOS, 8M:2G, 5M:5G, 2M:8G). Values normalized with respect to MTMOS.

In order to analyze the mineralization capacity, calcium deposits were evaluated using an osteogenic medium culture. Fig. 11 shows the quantification of these deposits using Alizarin Red S staining for each material at two culture times (7 and 14 days). The values were normalized with respect to MTMOS coating for easier determination of the influence of the GPTMS content.

Values of Alizarin Red presented big differences depending on the composition. Values of mineralization of MTMOS coatings were the lowest and formulations with GPTMS content presented higher mineralization values in the two test periods. After 7 culture days, MTMOS had the lower quantity of calcium, what can be related with the poor number of attached cells and the low Si release to the medium from this type of coating. When GPTMS was added to the formulation greater number of mineralized extracellular matrix was detected. Although the mitochondrial activity of 5M:5G and 2M:8G coatings decreased above 7 days of culture (Fig. 9). These coatings after 14 days of culture reached the maximum value of mineralization. For this time, the results of mineralization of GPTMS samples increased strong and independently of the composition.

Reffitt et al. [9] founded that physiological concentrations of Si in the form of orthosilicic acid stimulate collagen type 1 synthesis in human osteoblast-like cells and skin fibroblasts. Treatment with Si also enhanced osteoblastic differentiation (enhanced alkaline phosphatase activity and osteocalcin synthesis in the MG-63 cells). Si is also known to bind to glycosaminoglycan macromolecules and has been shown to play a role in the formation of crosslinks between collagen and proteoglycans [26] thus resulting in the stabilization of bone matrix molecules and preventing their enzymatic degradation. It is likely that the mechanism of action of Si in bone matrix synthesis may involve a complex biochemical set of interactions [27] with biological molecules and the high values of mineralization showed by GPTMS containing coatings indicate that this may be another possible mode of action of soluble Si.

Our results suggest that *sol–gel* coatings are able to produce Si release that can increase the differentiation process of the MSC onto osteoblastic cells, and so production of calcium deposits could be detected at 7 and 14 days.

3.6. *Biological characterization.* In vivo *study*

The good *in vitro* results obtained with GPTMS containing coatings leaded to select the 5M:5G coating to be tested under *in vivo* conditions. To study the tissue response to sol–gel coatings, biocompatibility, osseointegration and degradation coating capabilities were evaluated through light microscope histological study (Fig. 12). *In vivo* Si release was observed by SEM images and EDX microanalysis (Fig. 13).

3.6.1. *Biocompatibility*

In order to evaluate biocompatibility of 5M:5G coating, three factors were kept in mind; bone marrow condition, presence/absence of foreign-body giant cells and fibrous capsule evolution. In the case of 5M:5G samples, bone marrow's architecture appeared modified with traumatic and aplasic tissue, particulary near the coating, at short periods. After, the architecture began to recuperate far of coating contact zone and, 8 weeks after implantation, bone marrow generally recovered the architecture and cellular charge, although not entirely.

Control samples showed normal bone marrow conditions after implantation with some traumatic signs after 4 weeks. However, after 8 weeks of implantation, bone marrow was recuperated. Foreign-body giant cells were found at all periods in case of control samples, but the number of cells did not exceed that of a normal foreign-body response. No foreign-body giant cells were found in case of 5M:5G. In all samples after 1 and 2 weeks of implantation a fibrous tissue relaxed (lax) band was found around the implants in medullar contact zones. After 4 weeks the fibrous tissue turned into a dense fibrous capsule. Moreover, at 8 weeks, a thick capsule was also observed between cortical bone and dental screw. In 5M:5G implants this capsule was found between trabecular bone and sol–gel coating, surrounding the implant.

3.6.2. *Osseointegration and* in vivo *coating degradation*

If cortical and trabecular bone repair in control implant and 5M:5G samples are compared, we could say that there is not a total osseointegration at cortical level neither in the case of the Ti control nor in the 5M:5G sample, because a thin fibrous layer appears between bone and screws. However, after 8 weeks of implantation, control screw osteoconduction allowed the new trabecular bone growth along its surface towards the endostium, getting a total osseointegration. Nevertheless, if we observe 5M:5G coated implants we have to say that they did not get a good osseointegration. First, a fibrous capsule surrounded the screw

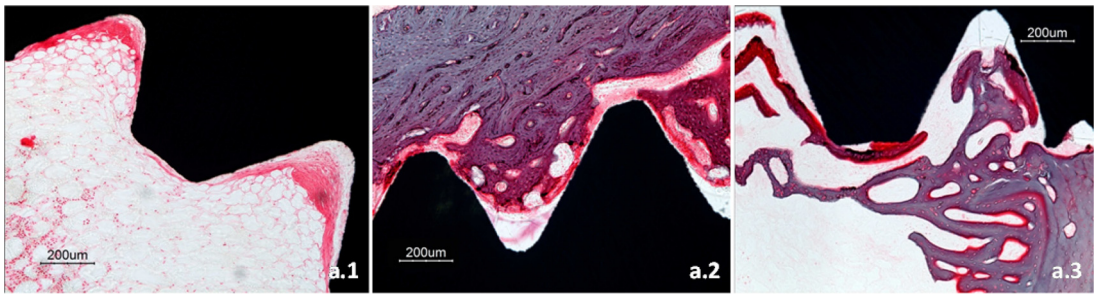

Fig. 12. Light microscopy images (10×) of 5M:5G *in vivo* samples after 8 weeks of implantation (a.1) recovery of bone marrow condition in implant distant zones and dense fibrous capsule with bone marrow contact, (a.2) fibrous capsule between bone and non resorbable coating and surrounding the screw to protect the bone marrow, (a.3) thin trabecular new bone without direct contact with 5M:5G sol–gel remaining coating (EXAKT® cut and Gomori Trichrome stain).

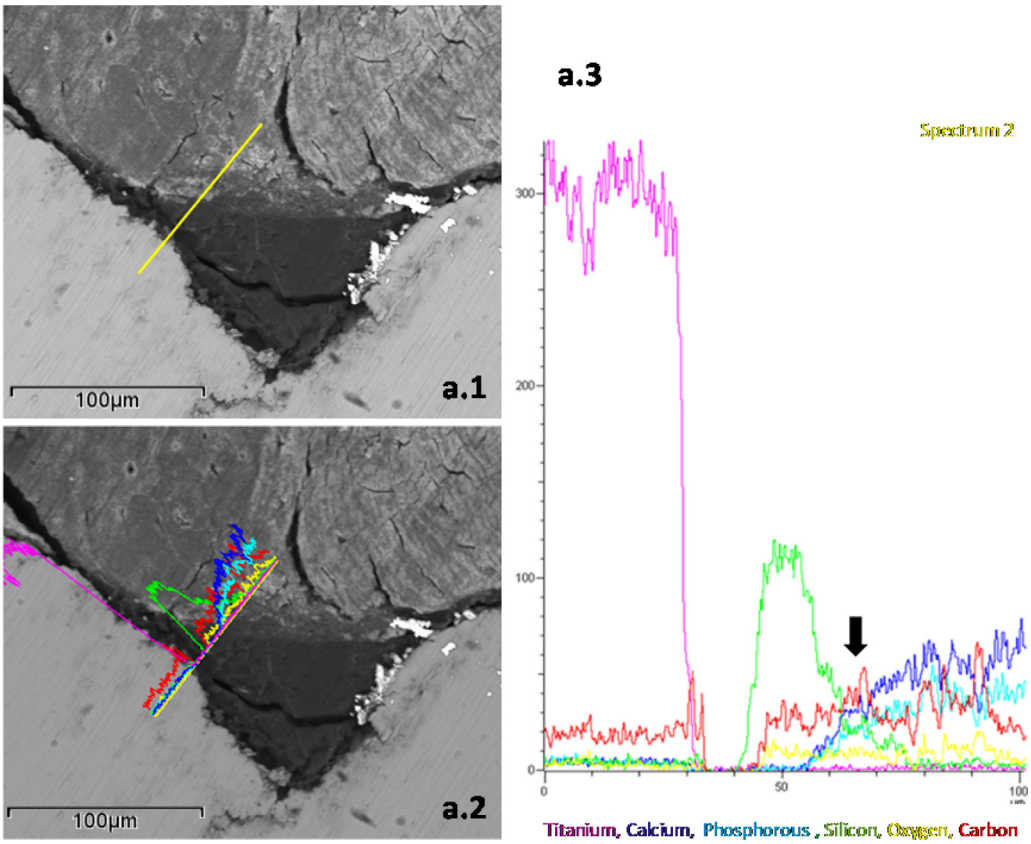

Fig. 13. (a.1, a.2) SEM images of *in vivo* 5M:5G interface after 1 week of implantation (1000×) and (a.3) EDX line profile crossing the different materials of the image, determining (from top to bottom); bone (Ca and P), an intermediate layer between coating and bone (Ca, P and Si), coating (Si), organic part of the coating (C) and titanium implant (Ti).

(Fig. 12a.1) and persisted between trabecular bone and coated implant (Fig. 12a.2). Second, a light level of osteoblastic activation was observed. Third, the architecture of the trabecular spicules formed was fine and slightly branched (Fig. 12a.3) and finally, a big part of the sol–gel coating remained in the threads until the end of the studied period in the trabecular zone as well as in the cortical zone (Fig. 12a.3).

3.6.3. In vivo *Si release*

In vivo Si release was studied by SEM image with EDX microanalysis and mapping of the histological samples (Fig. 13). A study was made analyzing the different elements signals: Si signal corresponding to sol–gel coating, Ca and P corresponding to bone, Ti corresponding to the implant and C corresponding to the organic part of the coating. The obtained images show a grey scale with a different grey colour for each zone, so that materials can easily be differentiated: light grey for Ti implant, dark grey for sol–gel coating and medium grey for bone.

Thus, for the 5M:5G coated implants, we observe various samples where Si, Ca and P signal coexisted in a same grey zone between bone and coating. This was detected in samples belonging to 1 week after implantation, in cortical and trabecular bone contact and in samples belonging to 2 weeks after implantation, in cortical bone contact. Therefore, a migration of Si in the bone is clearly observed indicating a biodegradation of the coating at 1 and 2 weeks after implantation, what could contribute to stimulate bone regeneration.

4. Conclusions

This study demonstrated that changes in the composition of the obtained *sol–gel* hybrid coatings highly influence their biodegradability and hence their biomedical applications.

An increase in GPTMS content increases the wettability and water absorption of the coating, due to either a decrease in the network crosslinking density of the hybrid material or the increase in the number of polar groups. The presence of GPTMS, which is a silicon precursor with a big organic group, contributes to hindering the Si—O—Si bond formation. Consequently, the degradability of the polysiloxane network in contact with water is higher due to the formation of a more open and hydrophilic network.

As a result, the addition of GPTMS to MTMOS, significantly increase the release of silicon compounds, which is reflected in a better AMSCs proliferation and mineralization. The fact of the formation of calcium rich deposits onto the coatings, suggests that the silicon compounds that are released during the degradation process of the material have *in vitro* osteoinduction ability. Nevertheless, *in vivo* behaviour of 5M:5G did not correspond with cellular results. Implanted coatings almost did not degrade, Si released was only detected by SEM-EDX, but thickness of coating did not reduce in time significantly.

Therefore, at the sight of the good cells behaviour *in vitro* associated to the presence of GPTMS, and taking into account the interest of obtaining materials with functional monomers we propose to carry out further research in these materials. In that case, the addition of a precursor which adds biodegradability to the coating, to enhance Si release from the earliest moments after

implantation should be a way to enhance the *in vivo* osteoinduction capability of the coating. Furthermore, the addition of active compounds attached to the GPTMS will be the next step of this research.

Acknowledgements

The supports of the Spanish Ministry of Economy and Competitiveness through project IPT-2012-0218-090000 and of the University of the Basque Country (UPV/EHU) through "UFI11/56" and "IT-611-13" are kindly acknowledged. We are especially thankful to D. Antonio Coso and D. Jaime Franco (Ilerimplant S.L., http://www.ilerimplant.com) for their cooperation.

References

[1] M. Manso-Silvan, C. Rodriguez-Navas, M.A. Hernandez, E. Lopez-Elvira, R. Gago, L. Vazquez, F. Agullo-Rueda, A. Climent, J.M. Martinez-Duart, J.P. Garcia-Ruiz, J. Biomed. Mater. Res. Appl. Biomater. 83B (1) (2007) 232–239.
[2] S.M. Hosseinalipour, A. Ershad-Langroudi, A.N. Hayati, A.M. Nabizade-Haghighi, Prog. Org. Coat. 67 (4) (2010) 371–374.
[3] M. Hernandez-Escolano, M. Juan-Diaz, M. Martinez-Ibanez, A. Jimenez-Morales, I. Goni, M. Gurruchaga, J. Suay, J. Sol–Gel Sci. Technol. 64 (2) (2012) 442–451.
[4] L. Ren, K. Tsuru, S. Hayakawa, A. Osaka, J. Sol–Gel Sci. Technol. 26 (1–3) (2003) 1137–1140.
[5] K. Tsuru, Z. Robertson, B. Annaz, I.R. Gibson, S.M. Best, Y. Shirosaki, S. Hayakawa, A. Osaka, Key Eng. Mater. 361–363 (Pt. 1, Bioceramics) (2008) 447–450.
[6] E.M. Carlisle, Science 178 (4061) (1972) 619–621.
[7] K. Schwarz, D.B. Milne, Nature 239 (5371) (1972) 333–334.
[8] X. Chatzistavrou, E. Kontonasaki, K.M. Paraskevopoulos, et al., 7 – sol–gel derived bioactive glass ceramics for dental applications, in: P Vallittu (Ed.), Non-Metallic Biomaterials for Tooth Repair and Replacement, Woodhead Publishing, 2013, pp. 194–231.
[9] P.E. Keeting, M.J. Oursler, K.E. Wiegand, S.K. Bonde, T.C. Spelsberg, B.L. Riggs, J. Bone Miner. Res. 7 (11) (1992) 1281–1289.
[10] D.M. Reffitt, N. Ogston, R. Jugdaohsingh, H.F.J. Cheung, B.A.J. Evans, R.P.H. Thompson, J.J. Powell, G.N. Hampson, Bone 32 (2) (2003) 127–135.
[11] Y. Shirosaki, K. Tsuru, S. Hayakawa, A. Osaka, M.A. Lopes, J.D. Santos, M.H. Fernandes, Biomaterials 26 (5) (2005) 485–493.
[12] S.I. Anderson, S. Downes, C.C. Perry, A.M. Caballero, J. Mater. Sci. Mater. Med. 9 (12) (1998) 731–735.
[13] M. Manso, S. Ogueta, P. Herrero-Fernández, L. Vázquez, M. Langlet, J.P. García-Ruiz, Biomaterials 23 (19) (2002) 3985–3990.
[14] C.J. Wilson, R.E. Clegg, D.I. Leavesley, M.J. Pearcy, Tissue Eng. 11 (1/2) (2005) 1–18.
[15] S.J. Garcia, J. Suay, Prog. Org. Coat. 59 (3) (2007) 251–258.
[16] S.J. Garcia, J. Suay, Prog. Org. Coat. 57 (3) (2006) 273–281.
[17] S.J. Garcia, J. Suay, Prog. Org. Coat. 66 (3) (2009) 306–313.
[18] A. Amirudin, D. Thierry, Prog. Org. Coat. 26 (1) (1995) 1–28.
[19] G.W. Walter, J. Electroanal. Chem. Interfacial Electrochem. 118 (1981) 259–273.
[20] E.P.M. van Westing, G.M. Ferrari, J.H.W. De Wit, Corros. Sci. 34 (9) (1993) 1511–1530.
[21] Peris Jl, J. Prat, R. Comín, R. Dejoz, I. Roger, P. Vera, Rev. Esp. Cir. Osteoart. 28 (1993) 231–238.
[22] J. Wierzchos, T. Falcioni, A. Kiciak, J. Wolinski, R. Koczorowski, P. Chomicki, et al., Micron 39 (2008) 1363–1370.
[23] O. Mahony, S. Yue, C. Turdean-Ionescu, J.V. Hanna, M.E. Smith, P.D. Lee, J.R. Jones, J. Sol Gel Sci. Technol. 69 (2014) 288–298.
[24] C.P. Stallard, K.A. McDonnell, O.D. Onayemi, J.P. O'Gara, D.P. Dowling, Biointerphases 7 (2012) 31.
[25] S.J. Garcia, M.T. Rodriguez, R. Izquierdo, J. Suay, Prog. Org. Coat. 60 (4) (2007) 303–311.
[26] K. Schwarz, Proc. Natl. Acad. Sci. 70 (5) (1973) 1608–1612.
[27] S.D. Kinrade, N.J.W. Del, A.S. Schach, T.A. Sloan, K.L. Wilson, C.T.G. Knight, Science 285 (5433) (1999) 1542–1545.